Preprints.org

Article

Not peer-reviewed version

Mass Production and Application of ^{17}O-Enriched Water Using Low-Energy Nuclear Reactions

Mou-Yung Liao , Sih-Li Chen , Li Xu , Yu-Hsiang Pan , Xin-Yuan Wu , Po-Hsien Wu , Jong-Fu Yeh , Yu-Yuan Hsien , Kuan-Che Lan , Yi-Tung Chen , TR Tseng , Fang-Wei Kang , Tan-Feng Tsai , Bin-Juine Huang *

Posted Date: 2 July 2026

doi: 10.20944/preprints202607.0090.v1

Keywords: ^{17}O-enriched water; ^{17}O isotopes; low-energy nuclear reactions

Article

Mass Production and Application of ^{17}O-Enriched Water Using Low-Energy Nuclear Reactions

Mou-Yung Liao [1], Sih-Li Chen [1], Li Xu [1], Yu-Hsiang Pan [2], Xin-Yuan Wu [2,6] , Po-Hsien Wu [2], Jong-Fu Yeh [2], Yu-Yuan Hsieh [2], Kuan-Che Lan [3], Yi-Tung Chen [4], TR Tseng [5], Fang-Wei Kang [5], Tan-Feng Tsai [5] and Bin-Juine Huang [1,6,*]

[1] Department of Mechanical Engineering, National Taiwan University, Taipei, Taiwan
[2] Advanced Thermal Devices (ATD), Inc., Konglin Group, New Taipei City, Taiwan
[3] Institute of Nuclear Engineering and Science, National Tsing Hua University, Hsinchu, Taiwan
[4] Department of Mechanical Engineering, University of Nevada, Las Vegas, Nevada, USA
[5] Mastek Technologies, Inc., New Taipei City, Taiwan
[6] Graduate Institute of Green Energy and Sustainable Technology, National Taiwan Normal University, Taiwan
* Correspondence: bjhuang38@gmail.com

Abstract

This study demonstrates the generation of excess energy and isotopes via Low-Energy Nuclear Reactions (LENR) of water in 11 reactors. Cross-verification using Mass Spectrometry (MS), Nuclear Magnetic Resonance (NMR), and Cavity Ring-Down Spectroscopy (CRDS) confirmed that ^{17}O production concurrently occurs with excess energy release, establishing the reproducibility of the LENR process. For mass production of ^{17}O-enriched water, a batch-type internal circulation system integrating a storage tank and a circulation pump was developed. This setup allows continuous manufacturing of ^{17}O-enriched water, with concentrations controlled via circulation time. Specifically, a 32 L system successfully yielded 30 mol% ^{17}O-enriched water within 290 h. For high-concentration measurement, a ^{17}O NMR-verified dilution method was established. Moreover, the LENR process induces the formation of stable, 200 nm nanobubbles (density: 9.33 x 10^6 particles/mL for reactor #185r12), predominantly composed of ^{17}O compounds of non-condensable gases (O_2 and CO_2). These persistent nanobubbles prevent gas loss, significantly enhancing the long-term storage stability and practical utility of the product. Utilizing this low-cost, mass-produced ^{17}O-enriched water, a preliminary MTT assay revealed that ^{17}O disrupts cancer cell metabolism, offering promising insights for future oncology research. Overall, this cost-effective mass-production technology facilitates the deployment of ^{17}O in healthcare and biomedical sectors, promoting further academic and clinical exploration.

Keywords: ^{17}O-enriched water; ^{17}O isotopes; low-energy nuclear reactions

---

1. Introduction

The phenomenon of cold fusion, initially reported in 1989 using deuterated heavy water as an electrolyte solution during electrolysis [1, 2], garnered widespread attention. Subsequent studies demonstrated that similar nuclear fusion-like phenomena could also be induced using light water (ordinary water) as the electrolyte [3–9]. Furthermore, anomalous energy yields have been observed in water-arc-induced fog generation [10], as well as during micron-sized droplet formation via electrohydrodynamic atomization (EHDA) of pure water [11]. These findings strongly imply that deuterated heavy water is not a strict prerequisite for inducing fusion-like phenomena, and that light water poses a viable alternative.

Our energy engineering research team has focused on investigating technologies that utilize cavitation in light water to generate excess heat via Low-Energy Nuclear Reactions (LENR). Our previous experimental findings [12] included calorimetric measurements of excess heat, as well as analyses of reactor failures caused by processing anomalies. Scanning Electron Microscopy (SEM) and Energy-Dispersive X-ray spectroscopy (EDX) cross-sectional evaluations confirmed that these failures were driven by nuclear transmutation. Subsequent experiments across a series of diverse reactors revealed that water can be excited to undergo nuclear reactions that yield excess energy. Concurrently, this process generates ^{22}Ne and ^{17}O isotope compounds, including $H_2{}^{17}O$, $^{17}O_2$, and $^{12}C^{17}O_2$ [13]. Because the ^{17}O isotope is generated as a low-cost byproduct of this energy-production process, its inherent medical value presents a compelling new frontier for clinical and biomedical applications.

To advance this technology, we have designed a variety of reactors to systematically explore how water cavitation can be leveraged to excite nuclear reactions and generate both excess energy and isotopic compounds [14]. In addition to utilizing mass spectrometry (MS) to analyze the effluents, we implemented nuclear magnetic resonance (NMR) spectroscopy and cavity ring-down spectroscopy (CRDS) for precise characterization. This paper presents our latest research on this topic, focusing on the reproducibility of the LENR phenomenon, product verification, the mass production of low-cost, high-concentration ^{17}O-enriched water ($H_2{}^{17}O$), and its associated concentration measurement techniques.

Recent advancements in quantum biology [16-18] suggest that because ^{17}O possesses a non-zero nuclear spin, its magnetic isotope effect (MIE) may influence free radical generation or cellular signaling pathways, thereby disrupting cancer cell metabolism and inducing apoptosis. Consequently, this mechanism holds potential for developing novel healthcare protocols or cancer therapies. However, the prohibitively high manufacturing cost of ^{17}O-enriched water has historically hindered clinical and translational evaluation. Utilizing the low-cost $H_2{}^{17}O$ mass-produced by our LENR reactors, we conducted preliminary *in vitro* MTT assays on cancer cells to provide a baseline reference for future medical applications.

2. Materials and Methods

2.1. Reproducibility of Low-Energy Nuclear Reactions (LENR) in Water

We have previously reported that cavitation in pure water can generate excess heat, and our mass spectrometry (MS) analysis of the resulting water samples revealed the presence of isotopes, thereby confirming that this phenomenon is driven by low-energy nuclear reactions [12, 13]. To verify the reproducibility of these findings, we designed and fabricated additional reactors for subsequent testing. Beyond measuring the excess heat yield (expressed as the coefficient of performance, COP_x), we employed multiple analytical techniques to characterize the effluents and validate the underlying nuclear reactions, including:

1. Mass Spectrometry (MS) Analysis: Conducted to determine the molecular and isotopic composition of the reaction effluents.
2. ^{17}O Nuclear Magnetic Resonance (^{17}O-NMR) Spectroscopy: Utilized to analyze and quantify the specific ^{17}O components within the generated products.
3. Cavity Ring-Down Spectroscopy (CRDS): Implemented for the high-precision detection and analysis of ^{17}O, ^{18}O, and D (deuterium) isotopes.

2.2. Reactor Design

To achieve high energy output efficiency, previous investigations utilized either a triple-pipe heat exchanger (VCS/THX series) that employed refrigerant vapor discharged from a refrigerant compressor to heat water, or a double-pipe heat exchanger (DHX series) that used boiler steam for water heating [12]. Although these two designs achieved remarkable thermal efficiencies ($COP_x > 4.2$), the highly intense LENR they induced led to an exceptionally short reactor lifespan (< 1 week). Due to their structural complexity and low reliability, these reactor configurations are impractical for real-world engineering applications such as power generation. To address these limitations, the present

Preprints.org (www.preprints.org) | NOT PEER-REVIEWED | Posted: 2 July 2026 doi:10.20944/preprints202607.0090.v1

study adopts a resonant cavity structure design, as shown in Figure 1. This new configuration facilitates large-scale scale-up while confining the cavitation phenomena to a region safely away from the reactor walls.

Figure 1. Schematic of the simplified LENR reactor.

2.3. Collection of Reaction Water

To facilitate the collection and subsequent analysis of the nuclear reaction products, the gas-liquid two-phase water flow discharged from the reactor is routed through an air-cooled radiator for heat dissipation. Upon reaching thermal equilibrium, the effluent condenses into stable liquid reaction water suitable for storage, utilization, or analytical testing, and is subsequently collected in a water tank, as illustrated in Figure 2.

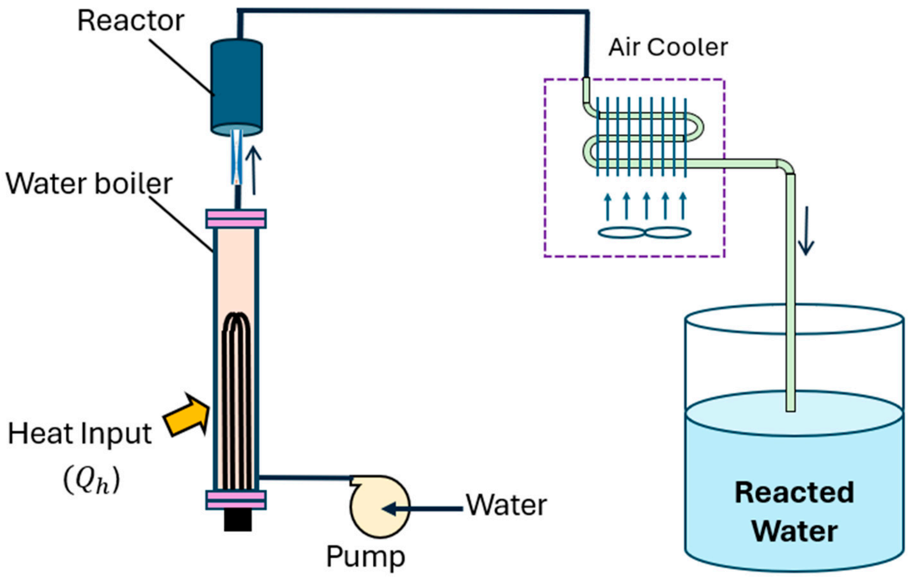

Figure 2. LENR system.

2.4. Gas Collection for Mass Spectrometry Analysis

The mass spectrometer employed in this study (Extorr XT300) is designed exclusively for gas-phase analysis; therefore, the reaction water stored in the reservoir must be converted into a gaseous state prior to measurement. The analytical results from mass spectrometry can be significantly influenced by sampling techniques and operational parameters, such as the vaporization process of the water sample, mass spectrometer inlet flow rates, system pressures, and interference caused by condensation. To ensure the consistency and reproducibility of the mass spectrometry measurements, a gas collection system, as illustrated in Fig. 3, was utilized along with a standard operating procedure (SOP) to convert the reaction water into water vapor. The sequential steps are outlined below:

 doi:10.20944/preprints202607.0090.v1

2.4.1. Temperature Control of Water Samples

The glass jar containing the water sample was connected to the gas collector, vacuum pump, valves, nitrogen cylinder, and air cylinder as illustrated in Figure 3. The glass jar was immersed in a constant-temperature water bath equipped with an electric heater and a stirrer, and a temperature controller was employed to maintain a constant temperature of 40 $\pm$1 °C.

2.4.2. Gas Collector Evacuation (Isolated from the Sample Jar)

The vacuum pump was turned on. Valves Vn and Va were closed, while valves Vg, Vs, and Ve were opened. Evacuation was conducted for at least 1 min before switching off the pump and closing Ve.

2.4.3. Gas Collection in the Collector (Connected to the Sample Jar)

Valves Ve, Vn, and Va were closed, while valves Vg and Vs were opened and maintained for 20 min. The vacuum state was utilized to vaporize the liquid water sample, allowing the water vapor to flow into the gas collector. The process was stopped by closing Vg and Vs once the gas pressure reached 30 torr.

2.4.4. Injection of 99.999% N_2

Valve Vn was opened until the pressure reached 630 torr. This step was primarily implemented to reduce the humidity of the collected gas, thereby preventing water vapor from condensing due to ambient temperature drops, which could otherwise interfere with the mass spectrometry operation.

2.4.5. Injection of Standard Air

Valves Va and Vg were opened, while Vn, Vs, and Ve were closed, and the process was stopped by closing Va and Vg when the pressure reached 760 torr. Because the concentration of ^{40}Ar in water is extremely low, the injection of standard air provided a sufficient amount of ^{40}Ar components to enhance the intensity of the m/z 40 internal standard signal in the mass spectrometer.

This gas collection procedure was optimized through extensive experimental experience. The connection between the gas collector and the mass spectrometer is shown in Figure 4. To ensure the consistency and reliability of the analytical results, this study simultaneously collected and compared the water after the LENR reaction with the unreacted background water (Reverse Osmosis water, RO water). The differences between the data sets obtained from both samples can be effectively utilized to determine whether additional components were generated by the nuclear reactions.

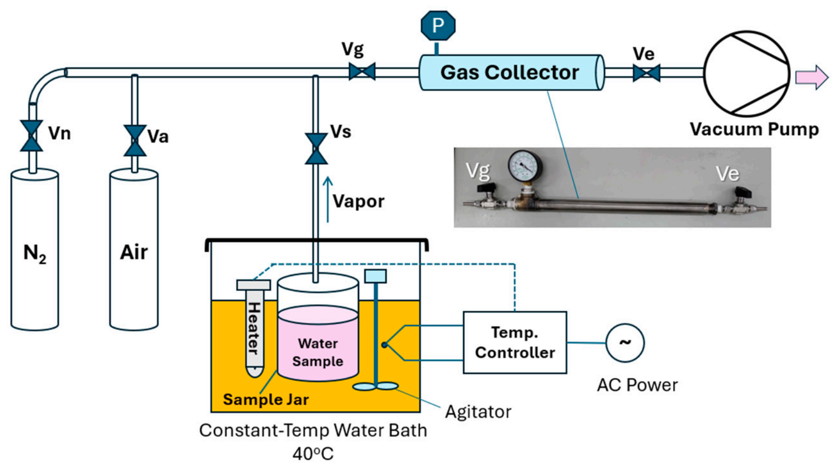

Figure 3. Gas collection system configured for reaction water vapor analysis.

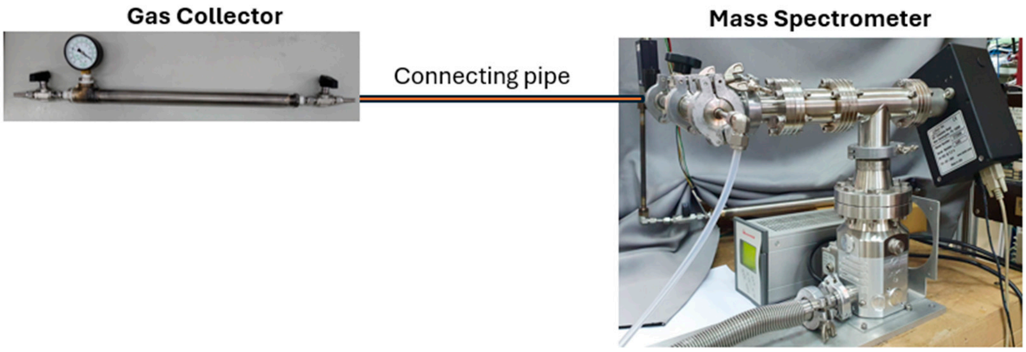

Figure 4. Experimental setup showing the connection between the gas collector and the mass spectrometer (Extorr XT300M).

2.5. Analytical Methods for the Composition (Qualitative) and Concentration (Quantitative) of LENR Products

Following the aforementioned vaporization and collection processes, both the reaction water obtained after the LENR process and the unreacted background RO water were introduced into a mass spectrometer (model: Extorr XT300M) for analysis. By comparing the resulting mass spectra with those of the unreacted water, it is possible to qualitatively determine whether the LENR process generated any anomalous or additional components.

2.5.1. Qualitative Analysis of Product Composition via MS

For non-condensable gases dissolved in water, *m/z* 40 was utilized as the internal standard, defined as follows:

$$I\# = \frac{m/z\ \#}{m/z\ 40};\ \ LL\#(gas) = \frac{I\#(gas)}{I\#(BG)}\ ; \qquad (1)$$

where # represents the mass number of the element, and BG denotes the unreacted water (background water). A value of LL#(gas) > 1.0 indicates that the LENR process generated elements in excess of those found in the background water.

For water isotopes in the liquid phase, such as $H_2{}^{17}O$, *m/z* 18 was employed as the internal standard (ordinary water), defined as follows:

$$L198(gas) = \frac{m/z\ 19}{m/z\ 18};\ \ LL198 = \frac{L198(gas)}{L198(BG)}\ ; \qquad (2)$$

Where BG denotes the unreacted water (background water). A value of LL198 > 1.0 indicates that the LENR process successfully generated m/z 19 elements ($H_2{}^{17}O$) exceeding the background water baseline.

To minimize experimental error, two water samples—the reaction water and the unreacted background RO water (BG)—were analyzed simultaneously. This dual-sampling approach effectively eliminates interference arising from variability in water quality.

2.5.2. Quantitative Analysis of Product Concentration via MS

The measured mass spectrometry signal intensity, I#, can be utilized to obtain a quantitative approximation of the concentration (expressed in mol%). Based on the definition in Eq. (1), I# represents the ratio of the mass-to-charge (*m/z*) signal of element # to that of ^{40}Ar. Within the linear range of the mass spectrometer, this ratio can be assumed to represent the concentration ratio of the two elements within the gaseous sample, given by:

$$I\# = \frac{m/z\ \#}{m/z\ 40} \approx \frac{C_x\#}{C_{40Ar}} \qquad (3)$$

Preprints.org (www.preprints.org) | NOT PEER-REVIEWED | Posted: 2 July 2026 doi:10.20944/preprints202607.0090.v1

where $C_x\#$ is the concentration of the element with mass number #, and C_{40Ar} is the concentration of ^{40}Ar in the gas sample. The gas sample in the gas collector was charged with water vapor (30 torr, pure nitrogen gas (630 torr), and standard air (100 torr, *Note: adjusted to match standard total atmospheric pressure of 760 torr*). Given that standard air contains ^{40}Ar at a concentration of 0.00934 (0.934 mol%), the concentration of ^{40}Ar within the gas sample is determined as:

$$C_{Ar40} = (130/760) \text{ x } 0.934 \text{ \%mol} = 0.16\text{\%mol} \qquad (4)$$

Consequently, the concentration of the target element can be calculated as:

$$C_x\# = I\# \text{ x } C_{40Ar} \qquad (5)$$

which can be explicitly determined from the measured value of I#. This estimation of non-condensable gas concentration remains valid provided that the operational parameters fall within the linear detection range of the mass spectrometer.

2.5.3. Qualitative Verification of ^{17}O Components in Water Samples via NMR and CRDS

The ^{17}O isotope can be detected and characterized utilizing ^{17}O Nuclear Magnetic Resonance (NMR) spectroscopy. To ensure cross-institutional validation and scientific rigor, the water samples in this study were submitted to three independent research facilities for analysis using three distinct ^{17}O -NMR spectrometers:

- **National Taiwan University:** Employed a Bruker AVIII HD 400 MHz spectrometer (A525, operating at 54.2 MHz) and a Bruker AVIII 400 MHz spectrometer (B662, operating at 54.2MHz).
- **National Central University:** Employed a Bruker AVIII HD 600 MHz spectrometer (operating at 81.37 MHz), conducted both with and without an inner tube configuration.
- **Rewave Tech Co (Bruker BioSpin), Ltd.:** Employed a Bruker AVIII HD 400 MHz NMR spectrometer.

Furthermore, isotopic verification was conducted using a Cavity Ring-Down Spectrometer (CRDS; Picarro L2140-i isotope analyzer) located at National Chung Hsing University, as structurally illustrated in Fig. 6.

Figure 5. Verification of ^{17}O isotopes using different NMR spectrometers.

 doi:10.20944/preprints202607.0090.v1

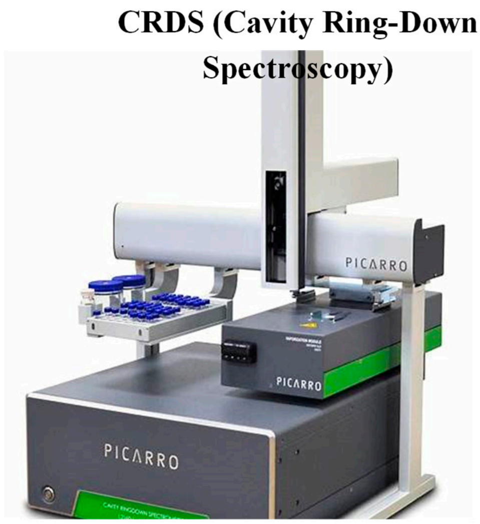

Figure 6. Isotopic product verification via CRDS: ^{17}O，^{18}O，D.

2.6. Enrichment and Mass Production of ^{17}O-Enriched Water

By incorporating a storage tank (capacity V) and a circulation pump into the LENR reaction configuration from Figure 2, a closed circulation system was constructed to continuously manufacture ^{17}O water (Figure 7). The accumulation of $H_2{}^{17}O$ content in the water volume V after each circulation loop can be determined via Equation (6), derived from Equation (2):

$$\text{LL198 - 1} = \frac{L198(gas) - L198(BG)}{L198(BG)} = \textit{The incremental increase in } H_2{}^{17}O \textit{ content per circulation cycle} \quad (6)$$

Figure 8 shows the concentration as a function of circulation cycles at LL198 = 1.6 (DEX-1Aa). With a 20 L batch size, reaching 20 mol% takes about 5 days (120 hrs).

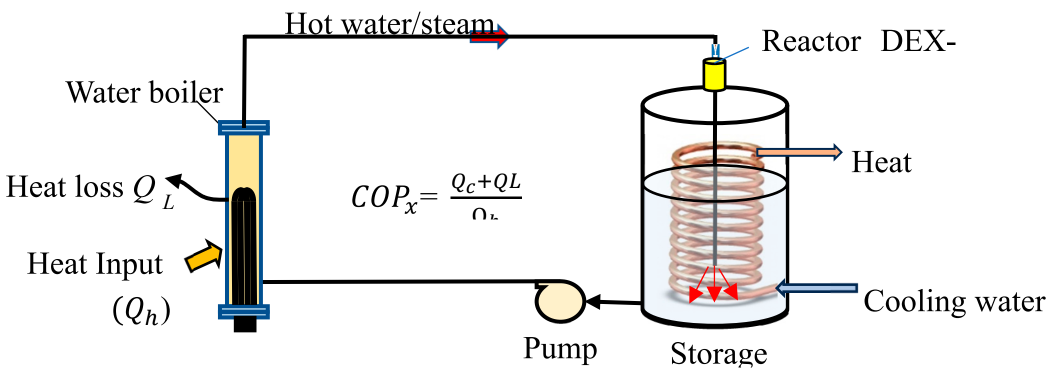

Figure 7. Experimental setup for the continuous mass production of ^{17}O-enriched water.

doi:10.20944/preprints202607.0090.v1

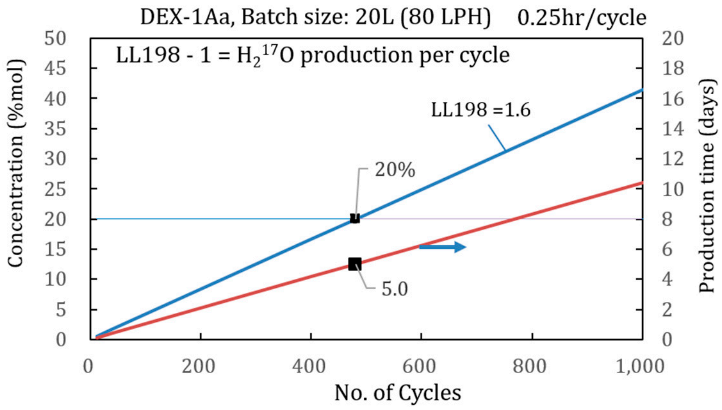

Figure 8. Relationship between concentration and time in mass production.

3. Results

3.1. Replication and Verification of LENR

Eleven distinct LENR reactors were designed and fabricated for the experiments. Water samples were collected both before and after the reactor treatments, and the samples were subsequently gathered according to the gas collection process illustrated in Figure 3. These gas samples were then subjected to Mass Spectrometry (MS) analysis to qualitatively determine and compare the composition of the reaction products. The results summarized in Table 1 reveal several noteworthy phenomena:

1. Excess ^{22}Ne consistently co-occurs with four ^{12}C-containing compounds and five ^{17}O-containing compounds, aligning with the conjectured nuclear reactions proposed in [12].

$$ {}^{1}_{1}H + e^{-} + \bar{\nu}_e + {}^{16}_{8}O \rightarrow \blacksquare \rightarrow {}^{17}_{8}O \tag{7} $$

$$ {}^{17}_{8}O + {}^{17}_{8}O \rightarrow \blacksquare \rightarrow {}^{12}_{6}C + {}^{22}_{10}Ne \tag{8} $$

2. For the two ^{17}O-containing CO_2 isotopologues, the MS index consistently follows the trend of LL45 > LL46, with the exception of reactors No. 10 and No. 11. This implies that the generation of a mono-substituted ^{17}O species in CO_2 via LENR is energetically more favorable than that of a di-substituted species.

3. For the two ^{17}O-containing O_2 isotopologues, the MS index always exhibits LL33 > LL34, implying that the generation of a mono-substituted ^{17}O species in O_2 via LENR is more favorable.

These results demonstrate the reproducibility of LENR, laying the foundation for the mass production of ^{17}O-enriched water.

Table 1. LENR replication results across eleven different reactors.

No.	Reactor	Gas Sample	COPx	Condition for LENR: COPx >1.05			^{17}O isotope compounds						^{18}O isotope compounds				
					^{22}Ne	CO_2	$H_2{}^{17}O$	$^{16}O^{17}O$	$^{17}O^{17}O$	$^{12}C^{16}O^{17}O$	$^{12}C^{17}O^{17}O$	$H_2{}^{18}O$	$^{17}O^{18}O$	$^{18}O^{18}O$	$^{12}C^{17}O^{18}O$	$^{12}C^{18}O^{18}O$
					LL22	LL44	LL198	LL33	LL34	LL45	LL46	LL20	LL35	LL36	LL47	LL48
1	RNJ-A1	**Tube64**	1.27	strong (>1.2)	3.82	2.71	**5.11**	1.12	0.99	2.73	2.43	1.11	2.58	1.24	1.48	1.53
2	nDJT-B	**Tube67**	1.21	strong (>1.2)	3.82	3.30	**6.58**	1.18	1.02	3.33	2.82	1.17	4.50	1.30	4.97	1.74
3	DEX-1(1)	**Tube69**	1.12	weak	1.09	0.75	**1.41**	0.99	1.01	0.84	0.81	0.98	2.40	1.41	1.81	0.98
4	JT2	**Tube70**	1.04	**No LENR**	**0.51**	**0.35**	**0.83**	**0.87**	**0.95**	**0.34**	**0.44**	**0.95**	**1.00**	**1.04**	**1.01**	**0.81**
5	VCS(5RT)	**Tube76**	1.65	strong (>1.2)	1.62	1.32	**6.88**	7.77	2.90	2.29	1.72	0.11	73.2	11.12	5.12	1.94
6	DEX-1(2)	**Tube81**	1.30	strong (>1.2)	4.17	1.06	**6.13**	4.04	1.58	6.48	3.63	4.70	9.12	1.87	4.19	2.61
7	DEX-1D	**Tube94**	1.12	weak	1.84	1.63	1.36	0.90	0.83	1.80	1.22	1.11	1.06	1.22	1.48	0.96
8	DEX-1Aa	**Tube96**	1.32	strong (>1.2)	1.64	1.62	1.32	1.13	0.96	1.93	1.01	1.11	1.14	1.07	1.42	1.06
9	JT5-A3V1	**Tube108**	1.20	strong (>1.2)	1.39	1.37	1.16	1.01	0.98	2.01	1.20	1.06	0.99	1.00	1.86	0.92
10	SRJ-5	**Tube111**	1.16	weak	1.17	1.01	1.54	1.19	0.99	1.21	1.46	1.11	1.86	0.98	1.48	0.79
11	**VCS(5RT)**	**Tube116**	1.60	strong	18.1	13.4	**15.6**	3.23	2.28	9.80	21.2	8.08	16.5	9.47	46.1	3.64

I## (gas) = m/z ##(gas) ÷ m/z 40 (gas); ##: mass number BG: background samples (unreacted RO water)
LL##(gas) = I##(gas)/I##(BG);
For water: L198 (gas) = m/z 19(gas) ÷ m/z 18(gas); LL198= L198(gas) / L198(BG)

 doi:10.20944/preprints202607.0090.v1

3.2. *Quantitative Verification of Product Concentrations via MS Analysis*

By analyzing the MS data using Equations (3)–(5), the concentrations of the reaction products can be estimated, as summarized in Table 2.

1. Sample **#178r3** was prepared using the configuration shown in Figure 7 and subjected to a total of 48 circulation cycles. Table 2 indicates that the concentrations of all detected gases are significantly higher than those in the untreated raw water.
2. ^{18}O is produced in the form of six distinct isotopic gases, which are dissolved in the water.
3. Among these isotopes, the species with the highest concentration is $^{17}O^{17}O$ (0.016 mol%), which represents pure isotopic oxygen.

Table 2. Concentrations of LENR products calculated from mass spectrometry data.

LENR Reacted Water (#178r3 from DEX-1Aa)	Contents	Concentration C_x (% mol)	Concentration ratio compared to unreacted water
$H_2{}^{17}O$ water	$H_2{}^{17}O$	2.49	66.3
$H_2{}^{18}O$ water	$H_2{}^{18}O$	0.96	47.3
Noble gas	^{22}Ne	2.14E-03	5.05
Regular O_2	$^{16}O_2$	3.67	1.22
Regular CO_2	$^{12}C^{16}O_2$	0.170	5.54
O_2 isotope compounds	$^{16}O^{17}O$	7.00E-03	2.92
	$^{17}O^{17}O$	0.016	1.34
	$^{17}O^{18}O$	2.64E-04	15.6
	$^{18}O^{18}O$	1.13E-03	2.25
CO_2 isotope compounds	$^{12}C^{16}O^{17}O$	2.87E-03	7.95
	$^{12}C^{17}O^{17}O$	1.30E-03	3.49
	$^{12}C^{17}O^{18}O$	1.17E-04	4.04
	$^{12}C^{18}O^{18}O$	3.29E-04	3.35

3.3. *Qualitative Verification of ^{17}O in Water Samples via NMR Spectroscopy*

The liquid water products collected from three reactors (DEX-1, DEX-1Aa, and VCS-5RT) operated under varied conditions were analyzed utilizing three distinct ^{17}O-NMR spectrometers across three independent organizations, and the findings were compared with the MS data. As summarized in Table 3, the results demonstrate high consistency among the different methods. This cross-verification robustly substantiates the MS findings, further confirming that excess ^{17}O is generated within the reactor via LENR.

Table 3. ^{17}O-NMR analysis of water samples.

	Sample	Tube 119	Tube 120	Tube 122	RO120	Tube 113	Tub 116	Tube112
	Reactor	DEX-1Aa 1 cycle	DEX-1Aa 2 cycle	DEX-1 24Co/60L	Unreacted RO Water (BG)	VCS(5RT) 50h/20L	VCS(5RT) 50h/10L	Unreacted Tap Water (BG)
NMR Model used	NMR Owner	**^{17}O-NMR signal area ratio relative to background (R)** [R > 1 denotes excess ^{17}O over the background]						
Bruker AVIII HD 400 MHz	National Taiwan University (NTU)	1.08	1.07		1.0		1.11	1.0
Bruker 400MHz	Rewave Tech Co (Bruker BioSpin)	1.04	1.03		1.0			
Bruker Ascend 600 HMz	National Central University (NCU)			0.98 (No LENR)		1.29	1.43	1.0
Mass Spectrometry **Peak signal ratio: LL198 = L198(gas) / L198(BG)** L198 (gas) = m/z 19(gas) ÷ m/z 18(gas) LL198 > 1 denotes excess $H_2{}^{17}O$ over the background (unreacted) water		1.63	2.42	1.00 (No LENR)	1.0	1.83	2.23	1.0

Preprints.org (www.preprints.org) | NOT PEER-REVIEWED | Posted: 2 July 2026 doi:10.20944/preprints202607.0090.v1

3.4. Isotopic Composition Analysis of Water Samples via CRDS

The third analytical technique employed for isotopic identification of the LENR products was cavity ring-down spectroscopy (CRDS). The $\delta^{17}O$, $\delta^{18}O$, and $\delta^{2}H$ values in the Tube116 and 190r1 samples reveal a significant enrichment of $^{17}O/^{16}O$, $^{18}O/^{16}O$ and $^{2}H/^{1}H$ ratios relative to the background (unreacted) water. Conversely, sample 185r12 exhibits enrichment exclusively in $^{17}O/^{16}O$ and $^{18}O/^{16}O$. Notably, as summarized in Table 4, these results demonstrate not only the expected synthesis of the ^{17}O isotope but also provide the first reports of anomalous ^{18}O and HDO enrichment in this system.

Table 4. CRDS identification of ^{17}O, ^{18}O, ^{2}H isotopes in water samples from different reactors.

Sample ID	Test run	$\delta^{17}O$ (‰) $H_2{}^{17}O$	Average $\delta^{17}O$ (‰)	$\delta^{18}O$ (‰) $H_2{}^{18}O$	Average $\delta^{18}O$ (‰)	$\delta^{2}H$ (‰) HDO	Average $\delta^{2}H$ (‰)
Tube 116 (VCS)	1st	-1.44		-2.76		-23.9	
	2nd	-1.41	-1.43	-2.72	-2.75	-24.2	-24.1
	3rd	-1.46		-2.78		-24.2	
Tube112 BG: Unreacted water	1st	-3.07		-5.87		-33.8	
	2nd	-3.07	-3.07	-5.85	-5.87	-33.8	-34.1
	3rd	-3.09		-5.91		-34.7	
Sample-to-BG Ratio			0.466		0.468		0.707
185r12 (DEX-1Aa)	1st	-3.5111		-6.7031		-37.1	
	2nd	-3.4653	-3.4653	-6.6144	-6.6274	-36	-36.3982
	3rd	-3.4195		-6.5647		-36.1	(no HDO)
185bg BG: Unreacted water	1st	-3.5751		-6.7841		-37.1	
	2nd	-3.5359	-3.5375	-6.7548	-6.7454	-36.6	-36.7338
	3rd	-3.5016		-6.6974		-36.5	
Sample-to-BG Ratio			0.980		0.983		0.991
190r1 (VCS707)	1st	-3.1696		-6.0215		-41.8	
	2nd	-3.1438	-3.1531	-6.0052	-6.0192	-42	-42.1053
	3rd	-3.1458		-6.0309		-42.5	
190bg BG: Unreacted water	1st	-4.0914		-7.7898		-48.6	
	2nd	-4.0462	-4.0516	-7.7377	-7.7431	-48.5	-48.6114
	3rd	-4.0172		-7.7017		-48.7	
Sample-to-BG Ratio			0.778		0.777		0.866

1) Instrument: Picarro L2140-I isotope analyzer (National Chung Hsing University, Taiwan).
2) Accuracy using long-term working standard (1 sigma): < 0.03 ‰, < 0.05 ‰, < 0.5 ‰ for $\delta^{17}O$, $\delta^{18}O$ and $\delta^{2}H$, respectively.
3) Conclusion: $\delta^{17}O$, $\delta^{18}O$, $\delta^{2}H$ in the samples of Tube116 and 190r1 reveal significant enrichment of $^{17}O/^{16}O$, $^{18}O/^{16}O$, $^{2}H/^{1}H$ as compared to the background/unreacted water. 185r12 reveals enrichment of $^{17}O/^{16}O$ and $^{18}O/^{16}O$ only.

3.5. Mass production of ^{17}O-enriched water

The LENR closed-loop circulation system configuration based on the DEX-1G reactor, as illustrated in Figure 7, was employed for the production of ^{17}O-enriched water. For a batch volume (V) of 32 L, the incremental increase in $H_2{}^{17}O$ content per cycle can be calculated using Equation (6). Continuous operation of the DEX-1G system for 290 hours (12 days) yielded 32 L of ^{17}O-enriched water with a concentration of 30 mol%, corresponding to an average daily production rate of 2.6 L. Furthermore, extending the operation to 480 hours (20 days) enables the synthesis of ^{7}O-enriched water with a concentration of 50 mol%, as demonstrated in Figure 9.

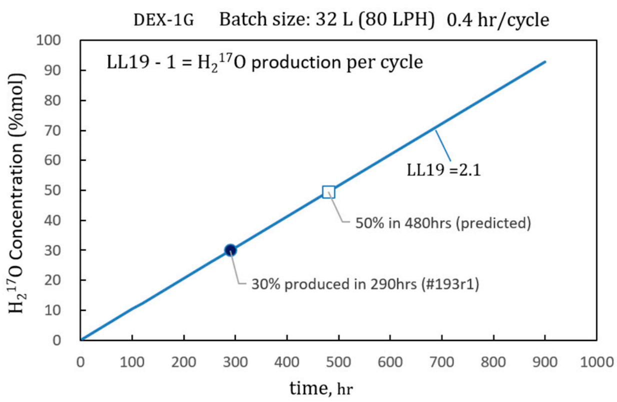

Figure 9. Mass production curve of DEX-1G.

3.6. Determination of ^{17}O-Enriched Water Concentration via ^{17}O-NMR Spectroscopy

The natural abundance of ^{17}O in natural water is 0.0375 mol%. Because the ^{17}O concentrations produced in this study exceed 5 mol% (more than 133 times the natural abundance), the precise determination of such high ^{17}O-enriched water concentrations is exceptionally challenging. To meet the quality control requirements for mass production, a dilution method was developed in this study to estimate the ^{17}O concentration. By analyzing the ^{17}O-NMR signals across various dilution factors (di), the dilution factor (diBG) at which the ^{17}O-NMR signal becomes identical to that of the background water (unreacted reverse osmosis [RO] water) can be identified. This specific dilution factor closely correlates with the concentration of the undiluted stock solution (C_x), which is expressed as follows:

$$C_x = \text{diBG} \times 0.0375 \text{ mol\% (natural abundance)}$$

Figure 10 presents the measured concentration of sample #190r1 (2.1 mol%).

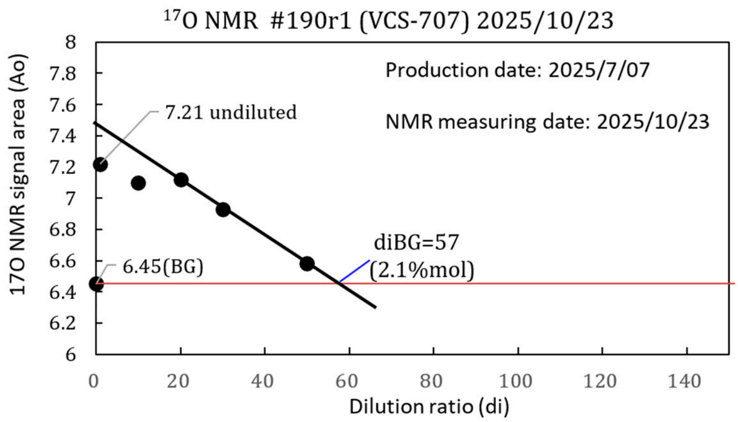

Figure 10. ^{17}O concentration measurement of sample #190r1.

Figure 11 presents the concentration determination results for sample #185r12 (30 mol%). Notably, sample #185r12 was obtained using the DEX-1Aa reactor with a water volume of 32 L, an operating temperature of 120°C, and a flow rate of 80 LPH across 485 continuous cycles (each cycle consisting of 40 minutes on and 60 minutes off). A high ^{17}O concentration of 30 mol% was achieved. Furthermore, this sample was analyzed after being stored at room temperature for nearly a year (10 months), demonstrating the excellent long-term stability of the water sample.

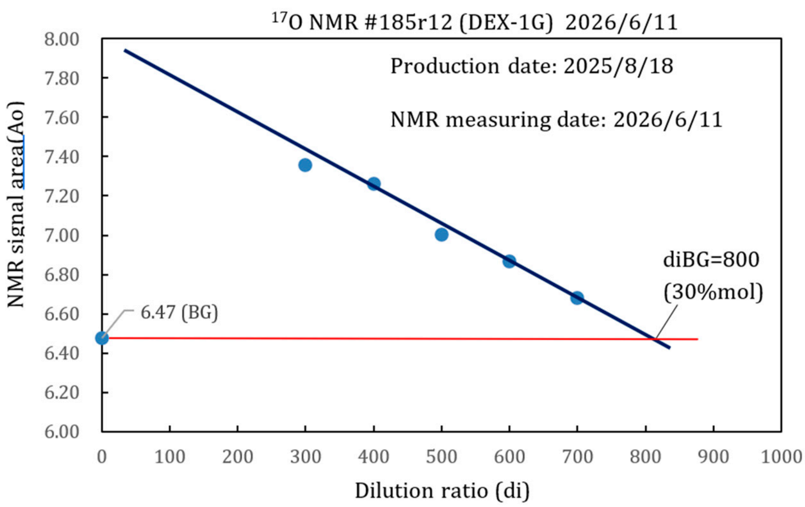

Figure 11. ^{17}O concentration measurement of sample #185r12.

3.7. Size Distribution Analysis of Bulk Nanobubbles in ^{17}O-Enriched Water

The ^{17}O-enriched water produced directly from the reactor is a liquid outflux that rapidly reaches a state of thermodynamic equilibrium with the bulk $H_2{}^{16}O$ water matrix. Notably, bubble evolution was observed during the LENR process. Nanoparticle tracking analysis (NanoSight) of sample #185r12 revealed a mean bubble diameter of 243 nm and a bubble density of 9.33 x 10^6 particles/mL (Figure 12). Following distillation of sample #185r12, the mean bubble diameter shrank to 119 nm, whereas the bubble density increased to 2.83 x 10^7 particles/mL (Figure 13). These nanobubbles are primarily composed of ^{17}O-containing compounds of non-condensable gases, such as O_2 and CO_2 (Table 2). Due to their nanoscale dimensions (Table 5), these bubbles remain highly stable within the aquatic matrix and resist conventional removal, thereby contributing to the long-term preservation stability of a portion of the ^{17}O isotopes. Consequently, ^{17}O-NMR characterization captures the superimposed sum of the ^{17}O signals from both the gaseous bubble and liquid phases, making it impossible to resolve their individual concentrations. This remarkable stabilization mechanism aligns with the framework proposed by Takahashi et al. [15], who reported that bulk nanobubbles (BNBs) achieve exceptional multi-month stability in aqueous solutions via a "condensed ionic cloud" that induces local precipitation, forming a topologically rigid solid nanobubble shell. Therefore, the gaseous ^{17}O components encapsulated within these nanobubbles are effectively preserved over extended periods, as validated by the long-term stability data of sample #185r12 presented in Figure 11.

Table 5. Particle size distribution of nanobubbles in sample #185r12.

Items	#185r12	#185r12 distilled
Mean (nm)	242.6 +/- 18.5	119.4 +/- 3.4
Mode (nm)	151.0 +/- 50.6	79.6 +/- 10.4
SD (nm)	178.3 +/- 16.9	77.2 +/- 12.8
D10 (nm)	72.5 +/- 10.8	43.7 +/- 5.9
D50 (nm)	180.5 +/- 23.8	101.5 +/- 2.4
D90 (nm)	498.6 +/- 35.4	204.4 +/- 10.2
Concentration (particles/mL)	9.33e+06 +/- 4.94e+05	2.83e+07 +/- 1.19e+06

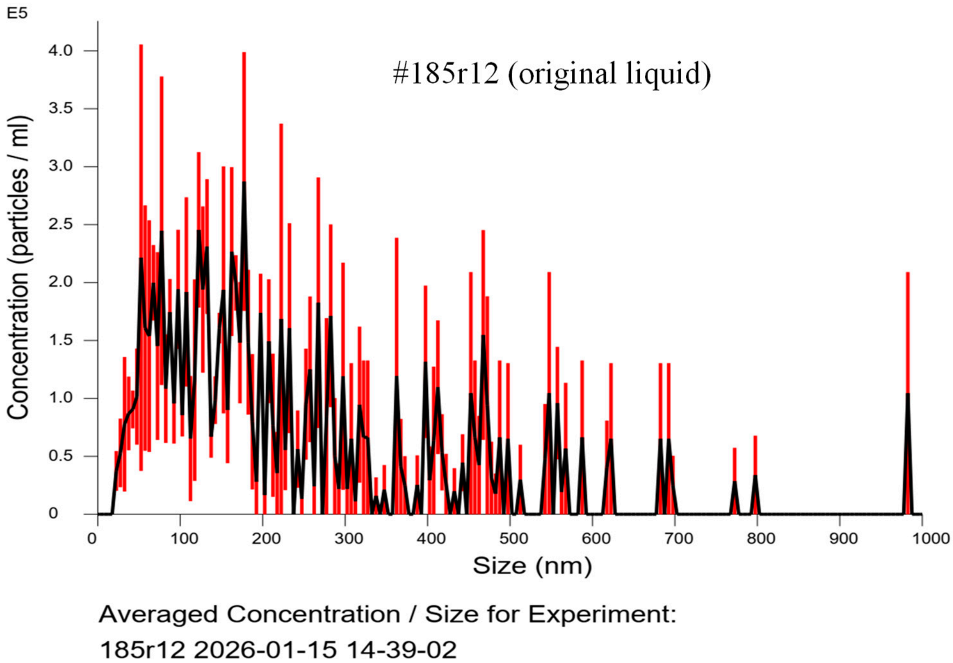

Figure 12. Bubble size distribution of sample #185r12 (original liquid).

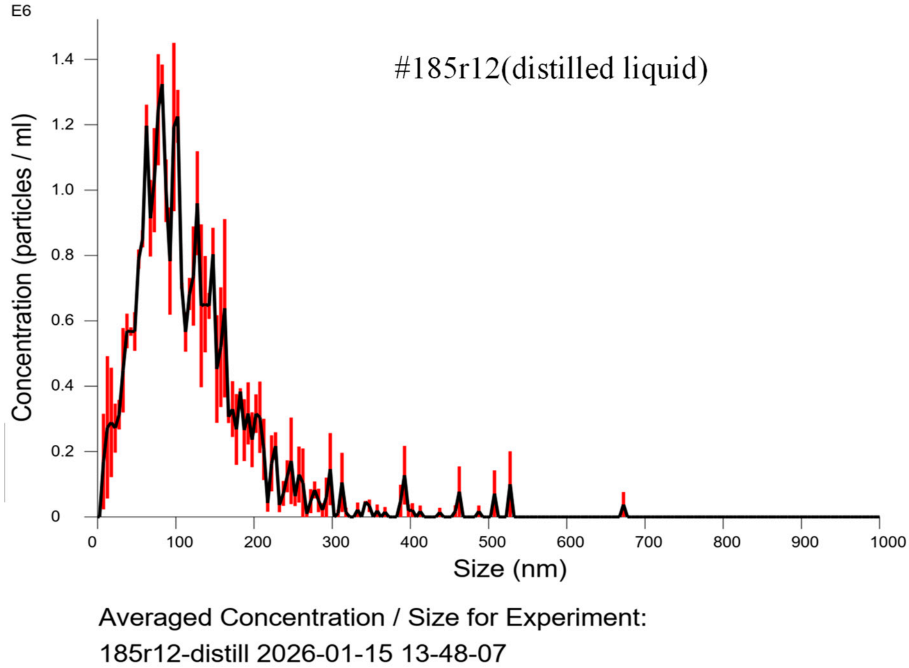

Figure 13. Bubble size distribution of sample #185r12 (distilled liquid).

3.8. MTT Assay Using ^{17}O-Enriched Water

Quantum biology studies suggest that ^{17}O may interfere with cancer cell metabolism [16–18]; however, experimental validation has been constrained by the scarcity of ^{17}O. In this study, an *in vitro* MTT assay was conducted on cancer cells using the mass-produced ^{17}O-enriched water.

A preliminary result from a cancer cell experiment (MTT) using 6 cells which shows that even low-dose ^{17}O-enriched water (0.35 %mol -Tube116) can alter metabolic activity in NG108 and B16F10 Cancer Cells as shown in Figure 14 [14]. NG108 cells consistently showed stable mild metabolic inhibition after treatment with 0.35% $H_2{}^{17}O$. For B16F10, mild cell activation was consistently observed. This may be caused by overclocking phenomenon [16,17] whose possible reaction curve can be like Figure 15.

Based on the preliminary MTT assay results, this study demonstrates that the low-cost, low-concentration ^{17}O-enriched water can interfere with the metabolic activity of cancer cells.

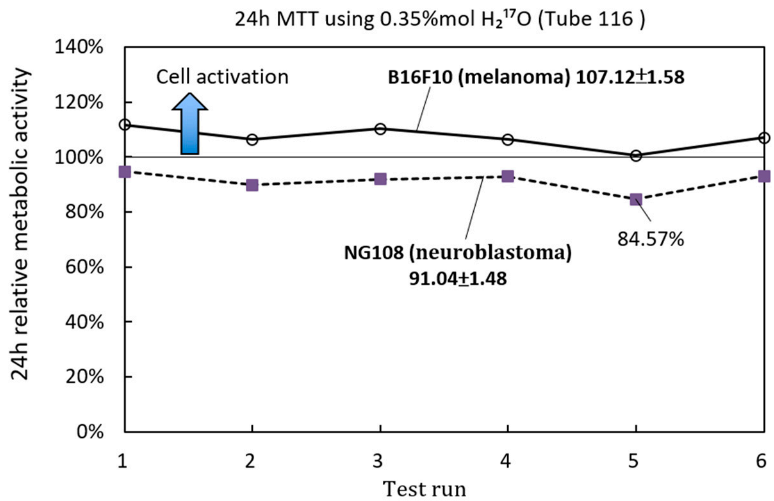

Figure 14. MTT assay of cancer cells treated with ^{17}O-enriched water.

Preprints.org (www.preprints.org) | NOT PEER-REVIEWED | Posted: 2 July 2026 doi:10.20944/preprints202607.0090.v1

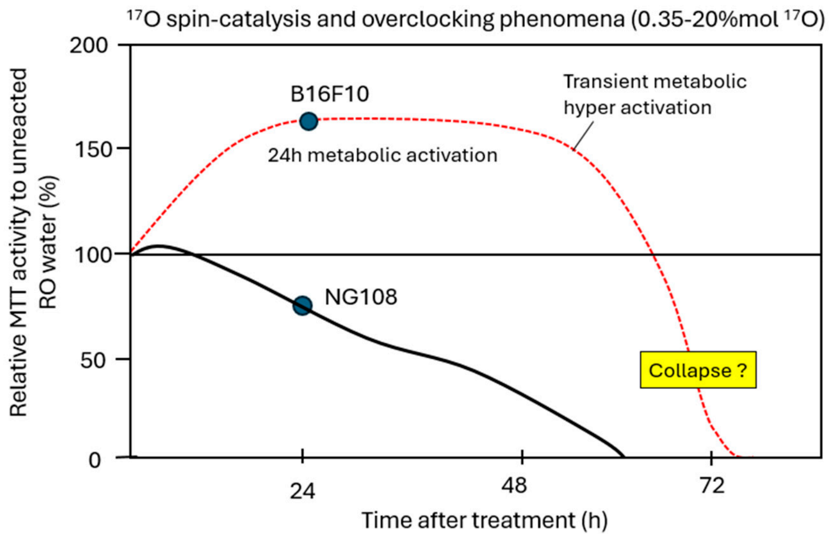

Figure 15. Hypothetical reaction curves corresponding to the overclocking phenomenon [16,17].

4. Discussions

In this study, experiments utilizing 11 independent reactor sets successfully demonstrated the reproducibility of water low-energy nuclear reactions (LENR) for the concurrent generation of excess energy and stable isotopes. By employing a multi-instrumental cross-verification strategy encompassing MS, NMR, and CRDS, the synthesized ^{17}O was confirmed to be synchronously generated with excess energy, thereby mitigating the measurement artifacts inherent in previous single-MS methodologies [13].

To transition this phenomenon from laboratory discovery to scalable manufacturing, a closed batch-type internal circulation system equipped with a storage tank and circulation pump was successfully engineered. This system achieves flexible concentration control over the produced ^{17}O-enriched water by modulating the circulation runtime. Specifically, the 32-L system benchmark established a high yield of 30 mol% ^{17}O-enriched water within 290 hours. Furthermore, to address the profound analytical challenges of quantifying such highly concentrated isotope samples, an innovative NMR-based dilution method was implemented, delivering precise determination.

Physiochemically, the reactor-yielded liquid $H_2{}^{17}O$ spontaneously reaches a thermodynamic equilibrium state with regular $H_2{}^{16}O$ water. Intriguingly, the LENR process also generates ultra-stable, bulk nanobubbles with an average diameter of approximately 200 nm and a concentration profile of 9.33 x 10^6 particles/mL. These nanoscale bubbles are predominantly composed of non-condensable gases (specifically ^{17}O-labeled O_2 and CO_2 complexes). Owing to their miniature dimensions and colloidal stability, these persistent bubbles resist standard physical removal, significantly promoting the long-term structural and isotope preservation stability of the $H_2{}^{17}O$ system. Although ^{17}O-NMR measurements evaluate the collective isotopic signals from both the liquid phase and encapsulated nanobubbles without individual distinction, the physiological efficacy remains pronounced. This ^{17}O-enriched matrix, featuring dense 200-nm nanobubbles, experiences minimal resistance when traversing cellular aquaporins (AQPs). Such heightened permeability facilitates effortless intracellular migration into the cell nucleus, stimulating critical metabolic pathways, advanced hydration, and internal detoxification in normal cells. Concurrently, the unique nuclear spin ($I = 5/2$) magnetic moment of ^{17}O is postulated to actuate the magnetic isotope effect (MIE) within key enzymatic cascades [16,17].

Utilizing the mass production of ^{17}O-enriched water, a preliminary MTT assay was performed on malignant cell lines. The resulting profiles verified that ^{17}O effectively interferes with cancer cell metabolism. This crucial milestone provides a foundational reference for downstream translational medicine, validating that our cost-effective, high-throughput LENR platform will drastically accelerate the implementation of ^{17}O-enriched water in subsequent therapeutic, oncology, and advanced healthcare frameworks.

5. Conclusion

This research conclusively validated the reproducibility of water LENR for isotope and thermal energy generation across 11 reactors. Through rigorous cross-examination using MS, NMR, and CRDS, the synchronous synthesis of ^{17}O alongside excess energy release was verified, resolving the single-MS analytical biases reported in historical literature [13]. The liquid effluent exists as a $H_2{}^{17}O$ matrix in thermodynamic equilibrium with standard $H_2{}^{16}O$ water, further characterized by persistent bulk nanobubbles containing non-condensable ^{17}O gas compounds (O_2 and CO_2). These highly degradation-resistant nanobubbles ensure reliable long-term isotope preservation. Ultimately, as an exceptionally economical and scalable byproduct of LENR, this specialized ^{17}O-enriched water opens up pioneering and highly accessible pathways for innovative medical applications, cellular metabolic regulation, and clinical oncological research.

Author Contributions: M.Y.L.: investigation, NMR data preparation, validation, data analysis. S.L.C.: project administration, resources, supervision. L.X.: conceptualization, methodology. Y.H.P.: investigation, data preparation, NMR validation, data analysis. X.Y.W.: investigation, data preparation, validation, data analysis. P.H.W: data preparation, validation, data analysis. J.F.Y.: conceptualization, methodology, investigation, project administration, supervision. Y.Y.H.: project administration, supervision. K.C.L.: supervision, validation. Y.T.C.: supervision, validation. T.R.T.: supervision, validation, MS data analysis. F.W.K.: supervision, validation, MS data analysis. T.F.T.: supervision , validation, MS data analysis. B.J.H.: conceptualization, methodology, investigation, project administration, supervision, resources, validation, data analysis, writing—original draft, funding acquisition. All authors have read and agreed to the published version of the manuscript.

Funding: This research work was supported by National Taiwan Normal University, National Taiwan University, National Tsing Hua University, ATD Inc., Mastek Technologies, Inc., Taiwan.

Data Availability Statement: Data will be made available on request.

Acknowledgments: The authors extend their appreciation to the researchers supporting this study.

Conflicts of Interest: The authors declare no conflicts of interest.

References

1. Fleischmann, Martin; Pons, Stanley. Electrochemically induced nuclear fusion of deuterium, Journal of Electroanalytical Chemistry and Interfacial Electrochemistry 1989, 261(2), Part 1, 301-308. https://doi.org/10.1016/0022-0728(89)80006-3. https://www.sciencedirect.com/science/article/pii/0022072889800063
2. Jones, S.; Palmer, E.; Czirr, J. *et al.* Observation of cold nuclear fusion in condensed matter. *Nature* **1989**, 338, 737–740 (1989). https://doi.org/10.1038/338737a0
3. Matsumoto, Takaaki. Cold Fusion Observed with Ordinary Water. *Fusion Technology*, **1990**, 17(3), 490–492. DOI: 10.13182/FST90-A29224
4. Notoya, R.; & Noninski, V. C. Excess heat during the electrolysis of a light water solution of K_2CO_3 with a nickel cathode. *Fusion Technology* **1992,** 21(1), 163–167.
5. Notoya, R. *Cold Fusion by Electrolysis in a Light Water-Potassium Carbonate Solution with a Nickel Electrode*. Fusion Technology **1993**, 24, 202–204.
6. Pinaev, A. V. (2005). The analyses of test data of cavitation heat-generator of TMK-25 type. In *Proceedings of the 13th International Conference on Condensed Matter Nuclear Science (ICCF-13)* (pp. 291–294). Sochi, Russia.
7. Pavlovoch Torchigin. (2024). *Nuclear Energy in Vortex Cavitation Generators*. ResearchGate. https://www.researchgate.net/publication/383093910
8. Kanarev, Ph. M.; Mizuno, T. (2003). Cold fusion by plasma electrolysis of water. Retrieved from https://www.researchgate.net/publication/237276063

 doi:10.20944/preprints202607.0090.v1

9. Ross, G.; Anwar, D.; Sedgwick, D.; Fustero, S. (2022). Experiments demonstrating the creation of elements via pulsed electric field in water and deuterated water: application to the production of fluorine. arXiv:2202.03744
10. Sundaresan R.; Bockris, J. O'm. Anomalous Reactions During Arcing Between Carbon Rods in Water. Fusion Technology **1994**, 26, 261-265.
11. Graneau, P.; Graneau, J.; Li, X. Renewable energy liberation by nonthermal intermolecular bond dissociation in water and ethanol. *Journal of Applied Physics* **2011**, 109(3), 034908. https://doi.org/10.1063/1.3544497
12. Huang, Bin-Juine *et al*. Excess energy from heat-exchange systems. *J. Condens. Matter Nucl. Sci.* **2022,** 36, 247–265. https://doi.org/10.70923/001c.72599
13. Huang, Bin-Juine *et al*. Water can trigger nuclear reaction to produce energy and isotope gases. Sci Rep. **2024,** 14(1), 214. https://doi.org/10.1038/s41598-023-50824-8. PMID: 38167629; PMCID: PMC10762109.
14. Huang, Bin-Juine; Liao, Mou-Yung; Pan, Yu-Hsiang *et al*. Replication of Low-Energy Nuclear Reaction in Water. The 26th International Conference on Condensed Matter Nuclear Science. 26-30 May, 2025, Morioka, Japan. https://www.researchgate.net/publication/392160175_Replication_of_Low-Energy_Nuclear_Reaction_in_Water
15. Takahashi, Masayoshi; Shirai, Yasuyuki; Sugawa, Shigetoshi. Free-Radical Generation from Bulk Nanobubbles in Aqueous Electrolyte Solutions: ESR Spin-Trap Observation of Microbubble-Treated Water. *Langmuir* **2021**, 37, 5005–5011 https://doi.org/10.1021/acs.langmuir.1c00469
16. Buchachenko, Anatoly L.; Kuznetsov, Dmitry. Magnetic Control of the DNA Synthesis by Nuclear Magnetic Ions of Mg, Ca and Zn as a Powerful and Universal Means to Kill Cancer Cells. *J Phys Chem Biophys* **2018,** 8(3): 1000272 (2018). doi: 10.4172/2161-0398
17. Koltover, Vitaly K. Magnetic isotope effects and nuclear spin catalysis in living cells and biomolecular motors: recent advances and future outlooks - Nuclear spin catalysis. *Biophysical Reviews* **2023**, 15:999–1006 https://doi.org/10.1007/s12551-023-01162-6
18. Little, Reginald B. On the Atomic Carcinogenic Mechanism and Cure for Cancer: Ferrochemistry for Cause of Warburg Effect, 27 October 2022 , 1-185 https://doi.org/10.9734/bpi/mono/978-93-5547-919-8